**ORIGINAL ARTICLE**

# Adaptive fuzzy controlled hybrid shunt active power filter for power quality enhancement

Alok K. Mishra[1] · Prakash K. Ray[2] · Ranjan K. Mallick[1] · Asit Mohanty[2] · Soumya R. Das[3]

## Abstract

A novel switching pulse generation methodology based on adaptive fuzzy hysteresis current controlled hybrid shunt active power filter (A-F-HCC-HSAPF) is presented in this paper for compensating reactive power and harmonics in distribution network. The harmonic problems are mainly evolved because of extensive use of nonlinear loads in industry and domestic sectors. There are some adverse effects of harmonics such as: malfunctioning of sensitive equipment, resonance issues, conductors heating, power losses and reduced efficiency in distribution system. To mitigate harmonics issues passive, filters are used but when the harmonic component increases the design of passive filters is complex and becomes bulky. With the advancement in power electronic, the active power filter has been designed. Generally, the rating of the active filter is very high for some applications; hence hybrid shunt active power filter (HSAPF) is proposed by low-rated shunt active power filter (SAPF) and low-cost shunt passive filter. Proportional-integral or fuzzy logic controller is used to estimate the reference current and to regulate the dc capacitor voltage. To generate the switching pulse for the voltage source inverter of the SAPF, a novel adaptive fuzzy hysteresis current controller (A-F-HCC) is adopted. The performance of the proposed A-F-HCC-HSAPF is investigated during steady-state and transient conditions using MATLAB/Simulink and real-time environments.

**Keywords** Adaptive fuzzy hysteresis current controller · Harmonic compensation hybrid shunt active power filter · Power quality

## 1 Introduction

Nowadays the improvement in power quality (PQ) is an important challenge in the field of power distribution system. Generally, the devices used in the load end such as switched mode power supply (SMPS), arc furnaces, uninterruptible power supply (UPS), adjustable speed drives (ASDs), and other power electronic devices are nonlinear in characteristics. These loads are the cause of different PQ problems including harmonics in source/load voltages and currents which badly affect the system efficiency, security, and reliability [1]. Therefore, many research works are carried out using different custom power devices (CPD) for improving the PQ of the system. The simplest and economical solution is the use of passive filters (PFs) [2] for PQ improvements. But, the PFs are sometimes become ineffective due to their large size, tuning and resonance issues, and fixed compensation characteristics [3]. Therefore for overcoming these issues, a new power electronics-based device called active power filters (APFs) is developed. APF injects the compensating current with equal magnitude and opposite sign in order to cancel out the harmonics to improve power quality [4, 5].

A series APF that compensates distortions in load voltage and current, by using an integrated quality controller (IQC), is presented in [6]. Authors in [7] eliminate the load current harmonics by using different inverter-based APF. The capability of APF depends upon the fastness and accuracy in generating the reference current and

✉ Prakash K. Ray
  pkray@cet.edu.in

1 Department of Electrical and Electronics Engineering, ITER, SOA University, Bhubaneswar, Odisha, India

2 Department of Electrical Engineering, CET, Bhubaneswar, Odisha, India

3 Department of Electrical Engineering, IIIT, Bhubaneswar, Odisha, India

switching pulses to the inverter. Hence, researchers have proposed many harmonics extraction techniques like *d-q*, *p-q* theory [8–11], adaptive filter [12], wavelet transform (WT) [13] and artificial neural network (ANN) [14] for improvement in power quality. But, the cost and rating of APF may increase with the increase in higher-order harmonics. Therefore, hybrid filter is designed by combining both passive and active filters to further enhance the compensation objective [15, 16].

In [17], the authors proposed a predictive direct power control technique to design SAPF for power quality improvement. Wiener filter with adaptive least mean square (ALMS)-based estimation is presented in [18] for compensation of harmonics. The authors in [19] have presented a fuzzy predictive control technique to mitigate harmonics. A new synchronous reference frame-based power angle control (SRF-PAC) technique [20] is suggested to design unified power quality controller (UPQC) for efficient mitigation of harmonics. In [21], the authors proposed a robust extended Kalman filter (REKF) for estimation of harmonics. A dual *p-q* theory-based harmonic estimation technique is discussed in [22]. Again, hysteresis current control (HCC), sinusoidal pulse width modulation (SPWM) and space vector pulse width modulation (SVPWM) techniques in SAPF are implemented for improving power quality [23]. A sliding mode control (SMC)-based APF is proposed for compensation objectives [24]. A modified SMC is presented using fuzzy logic control (FLC) for harmonics mitigation [25]. The authors in [26] suggested a particle swarm optimization (PSO) and fuzzy logic controller for designing SAPF and adaptive sliding mode control-based neural network (ASMC-NN) [27] for PQ improvements are proposed by researchers. A fuzzy-PI-based current control algorithm is presented in [28], while FLC with PWM is presented in [29] for improvements of harmonics. Among the several current control algorithms, the HCC technique [30] provides quicker current controllability, faster response, peak current limiting capability and simple execution. However, the drawback of HCC is that, the variation of switching frequency is within a particular band which is unequal. To overcome these restrictions, an adaptive hysteresis current controller (AHCC) [31] is developed where the hysteresis band can be changed according to the parameters of supply and load to optimize the performance of the PWM inverter. But, the switching frequency in AHCC is very high due to which more switching loss will occur in the network.

Hence, a novel A-F-HCC technique [31] is proposed in this paper for regulating the modulation frequency, to reduce the switching loss, and hysteresis band can be made adaptive. The hysteresis bandwidth is calculated by FLC in the proposed method. Again, the voltage across dc link capacitor is regulated using PI or FLC [32, 33] for

extracting the amplitude of reference current. Compared to PI, the FLC is more robust [34] and does not need very detailed modeling for handling the uncertainty and nonlinearity. Extensive simulation and real-time experiments are carried out to test the robustness of the proposed SHAPF under different loading conditions.

In this paper, Sects. 2 and 3 provide the description of shunt passive and active filters, respectively. Section 4 presents precise strategy of the proposed HSAPF. The different control strategies to extract the reference current for SAPF are described in Sect. 5. Case studies using simulations and experiments are presented in Sect. 6, and conclusion is given in Sect. 7.

## 2 Shunt passive filter system

Shunt active filters provide a better solution for the harmonic mitigations. But, as the cost of the APF is higher, shunt passive filters are being used for many applications for providing a cost effective solution for harmonic mitigations. The passive filter connected in shunt has the ability to eliminate 5th-, 7th-, 11th-order harmonics. In this work, single-tuned 5th and 7th harmonic filter and double-tuned 11th and 13th harmonic filter are considered for designing the shunt passive filter (SPF). The single-line diagram of the SPF is displayed in Fig. 1. The design of single-tuned SPF and double-tuned SPF is discussed in the following subsections.
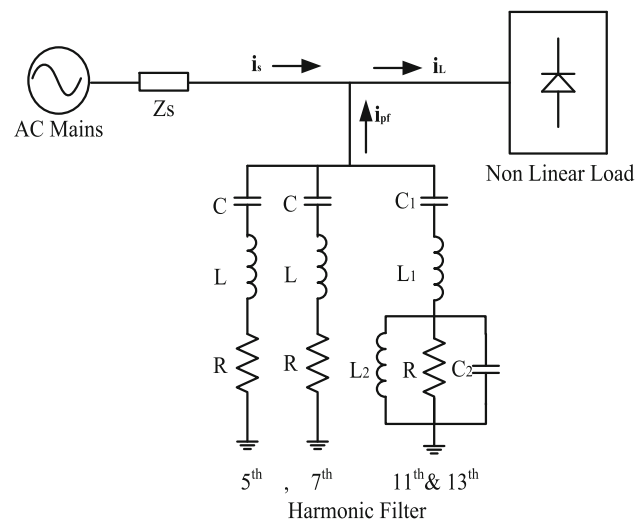


Fig. 1 Single-line diagram of the shunt passive filter

## 2.1 Design of single-tuned shunt passive filter (STSPF)

The impedance of a single-tuned filter is calculated as follows:

$$Z_{\text{filter}} = R + j\left(\omega L - \frac{1}{\omega C}\right) \tag{1}$$

Tuning frequency $f_{\text{tuned}}$ of the filter is given in (2)

$$f_{\text{tuned}} = \frac{1}{2\pi\sqrt{LC}} \tag{2}$$

In (3), $V_{\text{LL}}$ and $k\text{VAR}_{\text{filter}}$ represent the rated line voltage and filter reactive power capacity, respectively. Firstly, the capacitor size is defined for a power factor of desired value at rated line voltage and then the reactance value is calculated using (3).

$$X_c = \frac{V_{\text{LL}}^2}{k\text{VAR}_{\text{filter}}} \tag{3}$$

The mathematical formula for the quality factor $Q$ is given in (4) from which it is clear that $Q$ decides the filter resistance value. Then, Eq. (5) provides the parallel resonance frequency which is less than the tuning frequency where $L_s$ is the source inductance.

$$Q = \frac{\sqrt{LC}}{R} \tag{4}$$

$$f_{\text{resonance}} = \frac{1}{2\pi}\sqrt{\frac{1}{(L_s + L)C}} \tag{5}$$

## 2.2 Design of double-tuned shunt passive filter

The tuned frequencies $\omega_1$ and $\omega_2$ are chosen first in the design of double-tuned filter for a specified system voltage $V$ and reactive power $Q$ and then the parallel resonance frequency $\omega_p$ is chosen in between the tuned frequencies. Next, the series resonance frequency $\omega_s$ is evaluated from (6).

$$\omega_s = \frac{\omega_1\omega_2}{\omega_p} \tag{6}$$

Neglecting dielectric losses in the capacitor and reactor's resistance, the value of $C_1$ is evaluated as:

$$C_1 = \left(\left(\frac{\omega_f\left(\frac{\omega_p}{\omega_1\omega_2}\right)^2 - \frac{1}{\omega_f} +}{\left(\frac{\omega_f\left(\omega_1^2 + \omega_2^2 - \omega_p^2\right)\omega_p - \omega_1^2\omega_2^2}{\omega_1^2\omega_2^2(\omega_p^2\omega_s^2)}\right)}\right)\right)\frac{V}{Q} \tag{7}$$

wherein $\omega_f$ is the fundamental angular frequency and by solving Eq. (7), $L_1$ is evaluated as per (8):

$$L_1 = \left(\frac{\omega_p}{\omega_1\omega_2}\right)^2\frac{1}{C_1} \tag{8}$$

The value of capacitor $C_2$ is

$$C_2 = C_1\left(\left(\frac{\omega_1^2 + \omega_2^2 - \omega_p^2}{\omega_s^2}\right) - 1\right) \tag{9}$$

After evaluating the values of $C_1$ and $C_2$, the reactor $L_2$ is calculated from (10)

$$L_2 = \frac{1}{\omega_p^2 C_2} = \frac{1}{\omega_p^2 C_1}\left(\frac{\omega_1^2 + \omega_2^2 - \omega_p^2}{\omega_s^2}\right) \tag{10}$$

This is how the different parameters of the passive filter are evaluated for harmonics compensation.

# 3 Shunt active power filter system

The basic configuration of the SAPF is depicted in Fig. 2 where the SAPF filter is connected to the distribution system at the point of common coupling (PCC) through the filter inductance $L_c$. The function of $L_c$ is to filter out the distortions due to the inverter switching. A compensating current, of same magnitude and opposite sign, is injected by the filter at the PCC to cancel out the harmonic contents,

The source current is expressed as:

$$i_s(t) = i_L(t) - i_c(t) \tag{11}$$

The source voltage is given by:

$$V_s(t) = V_m \sin\omega t \tag{12}$$

If the load current is distorted, it can be expressed as:
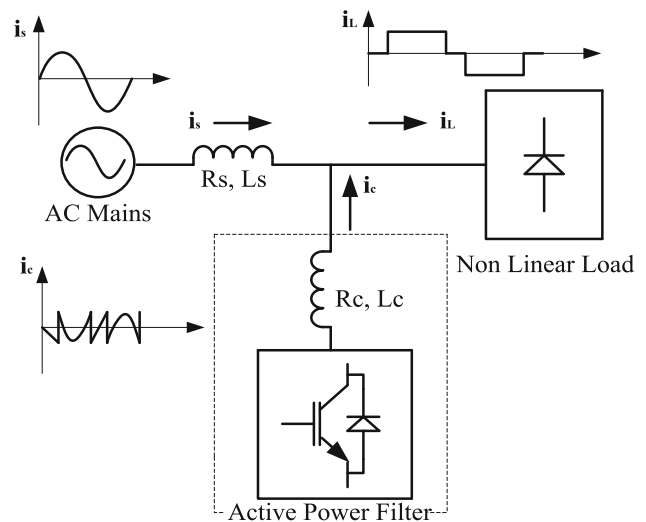


Fig. 2 Basic configuration of SAPF

$$i_L(t) = \sum_{n=1}^{\infty} I_n \sin(n\omega t + \phi_n)$$

$$= I_1 \sin(\omega t + \phi_1) + \left( \sum_{n=2}^{\infty} I_n \sin(n\omega t + \phi_n) \right) \quad (13)$$

The power across the load is expressed as:

$$\begin{aligned} p_L(t) = v_s(t) * i_L(t) &= V_m I_1 \sin^2 \omega t * \cos \phi_1 \\ &+ V_m I_1 \sin \omega t * \cos \omega t * \sin \phi_1 \\ &+ V_m \sin \omega t * \left( \sum_{n=2}^{\infty} I_n \sin(n\omega t + \phi_n) \right) \end{aligned} \quad (14)$$

$$p_L(t) = p_f(t) + p_r(t) + p_h(t). \quad (15)$$

here $p_L(t)$ consists of harmonic power $p_h(t)$, fundamental reactive power $p_r(t)$ and active power $p_f(t)$. From (14), the fundamental real power across the load is derived by

$$p_f(t) = V_m I_1 \sin^2 \omega t * \cos \phi_1 = v_s(t) * i_s(t). \quad (16)$$

For converting the source current $i_s(t)$ to pure sinusoidal form so as to make it in phase with the voltage, the SAPF provides the required reactive power compensation for which the three-phase source currents is given by

$$i_{sa}^*(t) = \frac{p_f(t)}{v_s(t)} = I_1 \cos \phi_1 \sin \omega t = I_{\max} \sin \omega t. \quad (17)$$

where $I_{\max} = I_1 \cos \phi_1$.

Similarly,

$$i_{sb}^*(t) = I_{\max} \sin(\omega t - 120°). \quad (18)$$

$$i_{sc}^*(t) = I_{\max} \sin(\omega t + 120°). \quad (19)$$

PI or FLC is used for regulation of dc link capacitor voltage of the inverter which in turn estimate the reference current $I_{\max}$ [32, 33].

# 4 Hybrid shunt active power filter (HSAPF)

HSAPF topology is designed by using a low-rated SAPF and a low-cost shunt passive LC filter. The proposed HSAPF has the merits of both active and passive filters, and eliminates the disadvantages of pure active and passive filters. Schematic diagram of HSAPF is shown in Fig. 3. The shunt-connected LC passive filter is comprised of single-tuned 5th and 7th harmonic filters and double-tuned 11th and 13th harmonic filters. The filtering characteristic is not satisfactory when passive filter is connected alone. Thus, APF is inserted into the existing passive filter configuration to improve the overall performance. SAPF operates as a current controlled voltage source and injects the compensation currents into the system. If only active filter is used, then the power rating required for PWM

converter is more. Hence, a hybrid combination of passive and active filters is used to mitigate the principal harmonics. To minimize the initial cost of the converter, power MOSFETs are used instead of IGBTs to form the PWM converter for low voltage applications. In this paper, compensation of harmonics and improvement in power factor is considered as the main objectives.

# 5 Control of SAPF

The basic configuration of the control strategy used for SAPF is depicted in Fig. 4. The proposed control structure can be divided into two parts out of which first one is extraction of reference current which is done by dc link capacitor voltage regulation using PI or FLC. The second part is the generation of switching pulse by PWM technique using fixed hysteresis, adaptive hysteresis and adaptive fuzzy hysteresis controller.

## 5.1 Extraction of reference current

SAPF compensates the distortions in the source current so that it can be in phase with the supply voltage without depending on the load current characteristics. Hence, in this method, the main currents are evaluated by calculating the three phase supply current:

$$\begin{aligned} i_{sa}^*(t) &= I_{\max} \sin \omega t \\ i_{sb}^*(t) &= I_{\max} \sin(\omega t - 120°) \\ i_{sc}^*(t) &= I_{\max} \sin(\omega t + 120°) \end{aligned} \quad (20)$$

In this equation, the peak value of the source current $I_{\max}$ and the phase are calculated. The phase of the source current is evaluated from the supply voltage and thus only the peak value $I_{\max}$ has to be calculated using PI or fuzzy logic controllers by the regulation of the voltage of the dc link capacitor.

There are two basic functions of the dc link capacitor of the inverter. During the steady state operation, it controls the dc link voltage with negligible distortions and during the transient operating conditions; it supplies the deficiency in the real power. During the steady state, the dc link capacitor voltage is maintained constant at the reference value because the supply and the real power demand are same. But, the balance between the supply and demand is affected by any sudden load switching or transient, thereby forcing the dc link capacitor to supply the deficient power. During such conditions, the capacitor voltage deviates from the desired reference value. To stabilize the voltage, supply current and hence the real power changes so that a balance between supply and load is maintained. Once the transient is over, the capacitor regains its original reference to reach

**Fig. 3** Schematic diagram of HSAPF
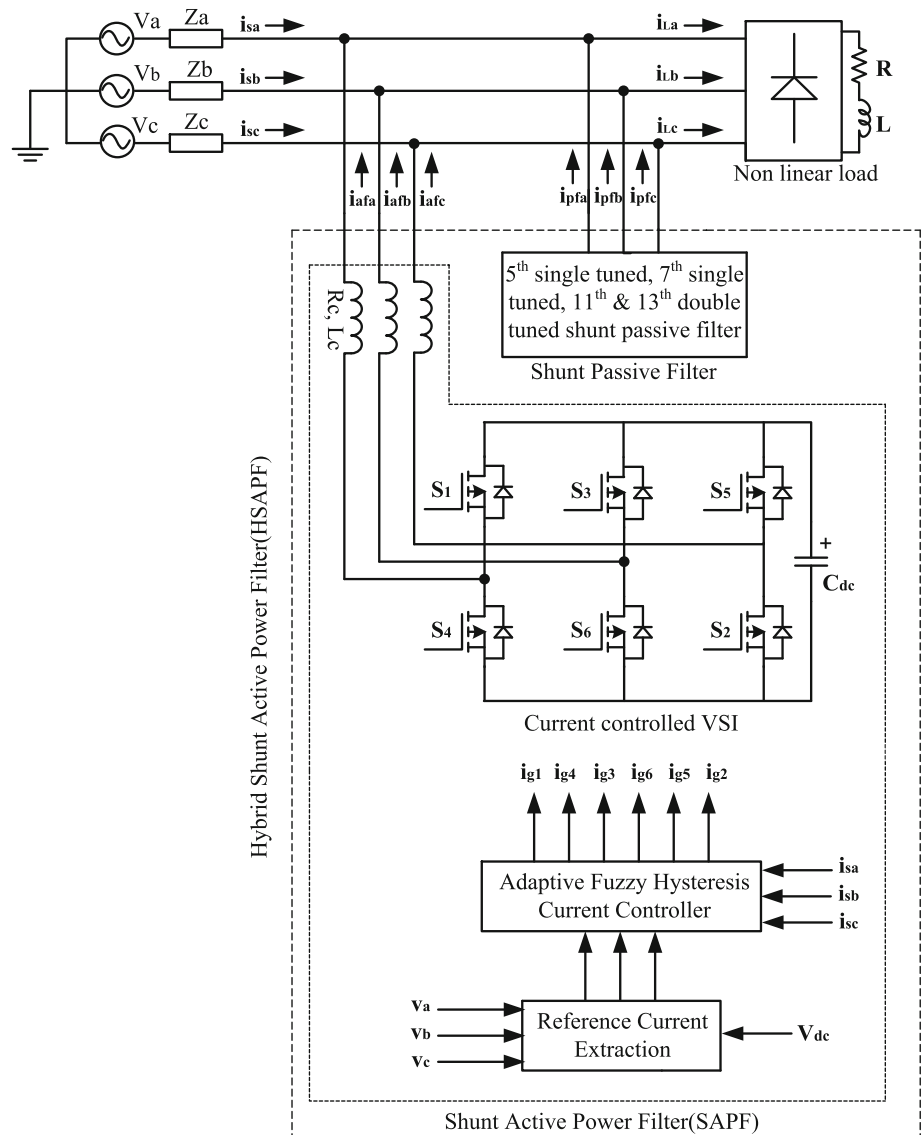


**Fig. 4** Configuration of the control strategy for SAPF
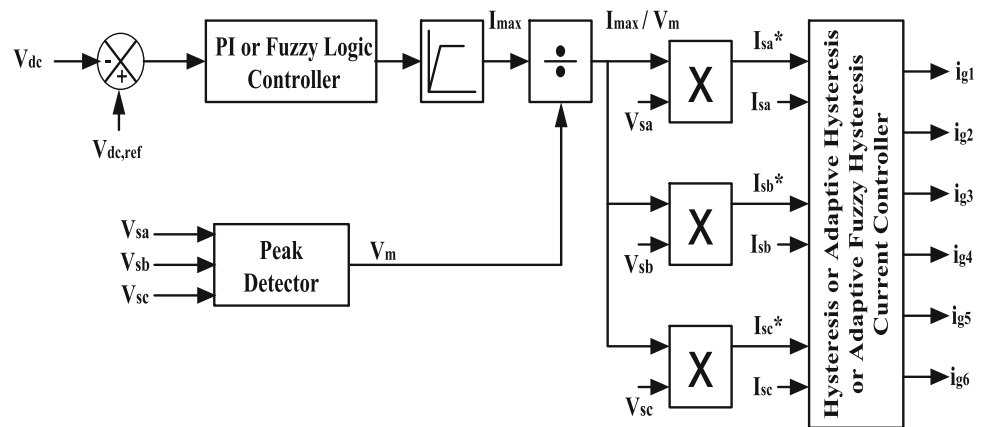


a new steady state. Hence, it is important to estimate $I_{max}$ to stabilize voltage across the dc link capacitor. With the above concept, it is easier to design the control circuit independent of the load current parameters. Hence, reference current is extracted using the conventional PI and the

proposed FLC for simpler implementation requiring less hardware circuitry.

### 5.1.1 PI controller

The input to the PI controller is the voltage error signal ($e$) between $V_{dc}$ and $V_{dc,ref}$, the actual and reference voltages of the dc link capacitor, respectively.

$$e = V_{dc,ref} - V_{dc} \qquad (21)$$

To attenuate the harmonic components, the error signal $e$ is passed through a low pass filter. The transfer function of the error signal is given as [31]:

$$H(s) = K_p + K_I/s \qquad (22)$$

The proportional and integral gains $K_p$ and $K_I$ are evaluated using (23) and (24), respectively, where $\xi$ (= 0.707) is the damping ratio and $\omega_n$ is the undamped frequency. The proportional and integral controllers eliminate the steady state error and the settling time of the dc link capacitor voltage. The PI controller is used to control the dc link capacitor voltage and estimates the peak current $I_{max}$. Then, $I_{max}$ is multiplied with the reference currents to produce the required gating pulse to the switches for injecting the compensating current at PCC.

$$K_p = 2 \cdot \xi \cdot \omega_n \cdot C \qquad (23)$$

$$K_I = \omega_n/2 \cdot \xi. \qquad (24)$$

### 5.1.2 Fuzzy logic controller (FLC)

The basic block diagram of the FLC for SAPF is depicted in Fig. 5. $V_{dc}$ and $V_{dc,ref}$ are sensed and compared to design the FLC for a SAPF. The error $e(n) = V_{dc,ref} - V_{dc}$ and change in error $ce(n) = e(n) - e(n-1)$ signals are used as inputs to the FLC.

*FLC is designed as follows:*

(a)  For each input and output variables, seven fuzzy sets (ENB, ENM, ENS, EZE, EPS, EPM, EPB) are defined.

(b)  Triangular membership functions are selected.

(c)  With the help of continuous universe of discourse, fuzzification is done.

(d)  Mamdani-type minimization operator is used.

(e)  Height method is used for defuzzification.

*Fuzzification*

From Fig. 5, the change in error and error, i.e. *ce(n)* and *e(n)*, are used input to the fuzzification process. Here, the numerical variables are converted to linguistic variables such as Error Negative Big (ENB), Error Negative Medium (ENM), Error Negative Small (ENS), Error Zero (EZE), Error Positive Small (EPS), Error Positive Medium (EPM) and Error Positive Big (EPB). Figure 6 gives the normalized triangular membership functions (MFs) used in fuzzification.

*Rule evaluator*

For evaluation of fuzzy set rules, some basic fuzzy logic operations, AND ($\cap$) for intersection, OR ($\cup$) for union and NOT ($-$) for complement, are used and defined as:

Intersection: AND: $\mu_{A \cap B} = \min[\mu_A(X), \mu_B(\chi)]$
Union: OR: $\mu_{A \cup B} = \max[\mu_A(X), \mu_B(\chi)]$
Complement: NOT: $\mu_A = 1 - \mu_A(\chi)$.

*Defuzzification*

The output generated by fuzzy logic rules are in linguistic variables and are converted to crisp values for real time requirements. This conversion procedure has to be conciliation between precision and intensity for computation.

*Rule and data base*

The description of the triangular MF is stored in the database that will be used by defuzzifier and fuzzifier. All the linguistic rules are kept in the rule base for designing FLC. All the 49 rules are formulated based on the expert's knowledge and depicted in Table 1.

The output of the FLC (i.e. $I_{max}$) and unit template reference currents are multiplied to generate the required reference current for mitigation of harmonics.



**Fig. 5** Fuzzy logic controller for SAPF
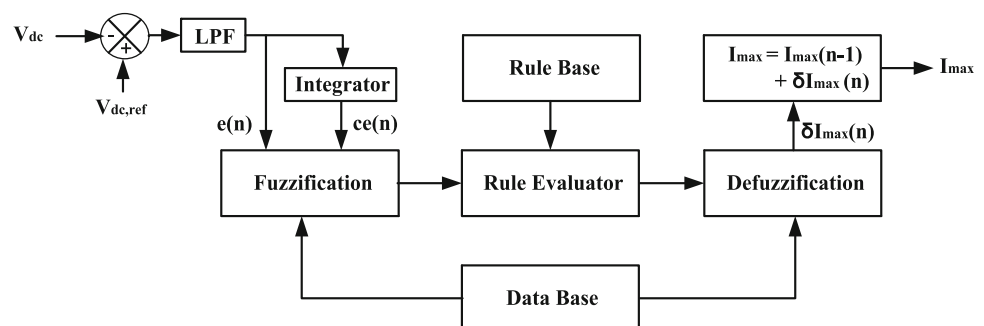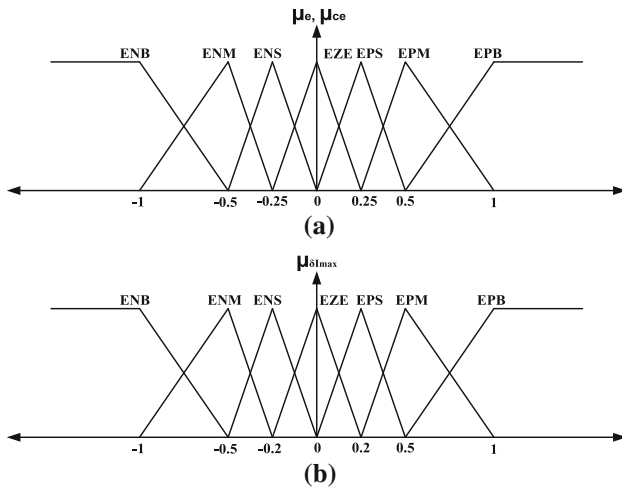
**Fig. 6** **a** MF for $e$ and $ce$ (input variables), **b** MF for $\delta I_{max}$ (output variable)

**Table 1** Rule base table

| e   ce | ENB | ENM | ENS | EZE | EPS | EPM | EPB |
|--------|-----|-----|-----|-----|-----|-----|-----|
| ENB | ENB | ENB | ENB | ENB | ENM | ENS | EZE |
| ENM | ENB | ENB | ENB | ENM | ENS | EZE | EPS |
| ENS | ENB | ENB | ENM | ENS | EZE | EPS | EPM |
| EZE | ENB | ENM | ENS | EZE | EPS | EPM | EPB |
| EPS | ENM | ENS | EZE | EPS | EPM | EPB | EPB |
| EPM | ENS | EZE | EPS | EPM | EPB | EPB | EPB |
| EPB | EZE | EPS | EPM | EPB | EPB | EPB | EPB |

## 5.2 PWM switching pulse generation/PWM current controller

The PWM current controller design decides the performance of the SAPF. When compared with other techniques such as SPWM and triangular current controller [34] for SAPF, Hysteresis Current Controller (HCC) has proven to be more suitable because of its merits like rapid current controllability, unconditional stability, fast response, good accuracy and simple in implementation [23]. The following subsections describe the fixed hysteresis, adaptive hysteresis and adaptive fuzzy hysteresis current controller for SAPF.

### 5.2.1 Fixed hysteresis current controller (FHCC)

The switching pulses generated by FHCC for SAPF are shown in Fig. 7 where $I_{ref}$ and $I_{actual}$ are the reference and actual current, respectively. They are compared, and the error is used to produce the gate pulse of the inverter. In a hysteresis controller, if the error signal is greater than upper band limit, the upper switch is made off and the

actual current starts decreasing. If error is more than the lower band limit, the upper switch is made on and the actual current starts increasing. The switching logic of the upper switch is expressed in (25).

$$S = \begin{cases} \text{OFF} & \text{if} \quad I_{actual} > I_{ref} + \text{HB} \\ \text{ON} & \text{if} \quad I_{actual} < I_{ref} + \text{HB} \end{cases} \tag{25}$$

In spite of many advantages, the main shortcoming of this control scheme is irregular switching frequency that causes audio frequency noise making the design of filter bit difficult [35].

The efficiency and reliability of the SAPF gets affected by this unpredictable switching frequency. The demerits of fixed hysteresis can be overcome by adaptive HCC where the bandwidth changes as per the variation in the instantaneous compensation current.

### 5.2.2 Adaptive hysteresis current controller (A-HCC)

The structure of the A-HCC is shown in Fig. 8. The switch $Q_1$ is turned ON and $Q_4$ is turned OFF when the current $I_a$ touches the lower hysteresis band. Hence, the current starts increasing when it touches the upper hysteresis band for which $Q_4$ is ON and $Q_1$ is OFF. Thus, the current starts decreasing touching the lower hysteresis band and the process repeats. During switching, $t_1$ and $t_2$ are evaluated using the following equations [36, 37].

$$\frac{di_a^+}{dt} = \frac{1}{L_c}(0.5V_{dc} - V_s) \tag{26}$$

$$\frac{di_a^-}{dt} = -\frac{1}{L_c}(0.5V_{dc} - V_s) \tag{27}$$

Now, we can write

$$\frac{di_a^+}{dt}t_1 - \frac{di_a^*}{dt}t_1 = 2\text{HB} \tag{28}$$

$$\frac{di_a^-}{dt}t_2 - \frac{di_a^*}{dt}t_2 = -2\text{HB} \tag{29}$$

$$t_1 + t_2 = T_c = \frac{1}{f_c} \tag{30}$$

where $f_c$ is the modulating frequency and $t_1, t_2$ are the switching interval, respectively. Adding (28) and (29) and substituting in (30), we get

$$\frac{di_a^+}{dt}t_1 + \frac{di_a^-}{dt}t_2 - \frac{1}{f_c}\frac{di_a^*}{dt} = 0 \tag{31}$$

Subtracting (29) from (28), we get

$$\frac{di_a^+}{dt}t_1 - \frac{di_a^-}{dt}t_2 - (t_1 - t_2)\frac{di_a^*}{dt} = 4\text{HB} \tag{32}$$

Putting (27) in (32)

**Fig. 7** Fixed-hysteresis band current controller
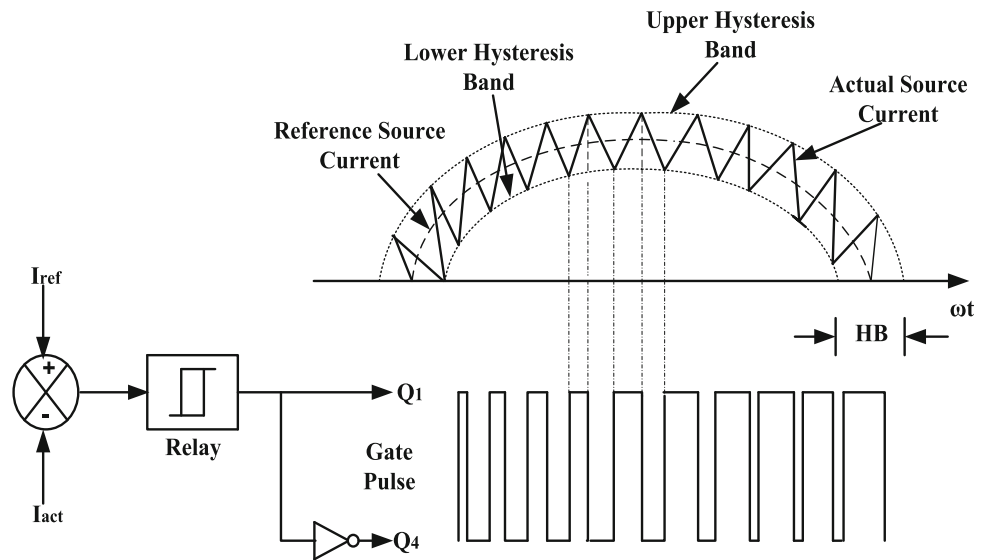


**Fig. 8** Adaptive hysteresis current controller (A-HCC)
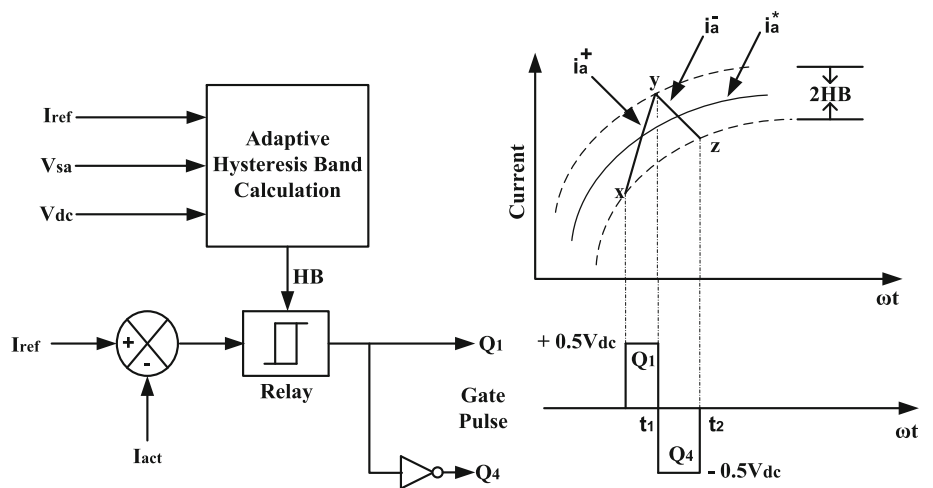


$$(t_1 + t_2)\frac{\mathrm{d}i_a^+}{\mathrm{d}t} - (t_1 - t_2)\frac{\mathrm{d}i_a^*}{\mathrm{d}t} = 4\mathrm{HB} \quad (33)$$

Putting (27) in (31) and after simplification

$$t_1 - t_2 = \frac{\mathrm{d}i_a^*/\mathrm{d}t}{f_c(\mathrm{d}i_a^+/\mathrm{d}t)} \quad (34)$$

Putting (34) and (26) in (33), simplifying we get

$$\mathrm{HB} = \left\{ \frac{0.125V_{\mathrm{dc}}}{f_c L_c} \left[ 1 - \frac{4L_c^2}{V_{\mathrm{dc}}^2} \left( \frac{V_s}{L_c} + m \right)^2 \right] \right\} \quad (35)$$

Here, $f_c$ is the modulating frequency and slope of reference current is represented by $m = \mathrm{d}i_a^*/\mathrm{d}t$. This controller keeps the modulating frequency $f_c$ nearly constant by changing the hysteresis bandwidth (HBW) at various points of fundamental frequency which in turn improves the switching of the inverter. From (35), it is clear that the HBW is a function of supply voltage, modulation

frequency $f_c$, dc link capacitor voltage $V_{\mathrm{dc}}$ and the slope of reference compensating current $m$. Adaptive HBW calculation block diagram is given in Fig. 9.

### 5.2.3 Adaptive fuzzy hysteresis current controller (A-F-HCC)

From Fig. 10, it is observed that the FLC is used for extremely efficient calculation of hysteresis bandwidth HBW′ in the proposed A-F-HCC. The difference between A-HCC and A-F-HCC is that, in A-HCC, the hysteresis bandwidth (HBW′) is evaluated based on Eq. (35), but the same bandwidth HBW in A-F-HCC is used as error signal E (HBW′) and change of error signal CE(HBW) for fuzzy logic processing. From Fig. 10, fuzzy logic controller output HBW′ is the adaptive fuzzy hysteresis current controller bandwidth. The fuzzy logic rules needed by the rule evaluator are stored as linguistic variables. To calculate the necessary bandwidth HBW′ in this adaptive fuzzy

**Fig. 9** Block diagram for adaptive HBW calculation
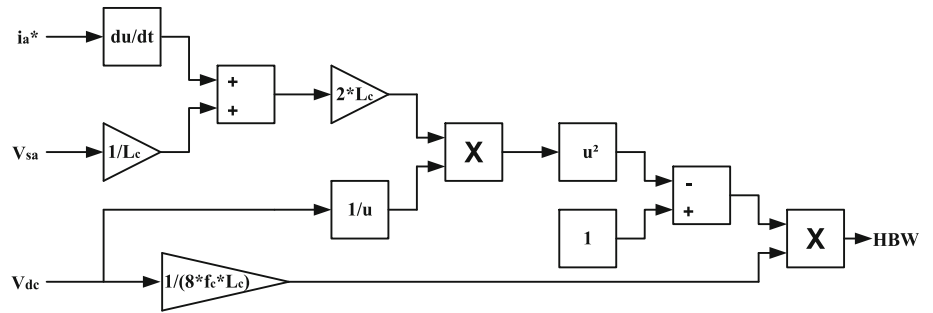


**Fig. 10** Structure of the proposed A-F-HCC
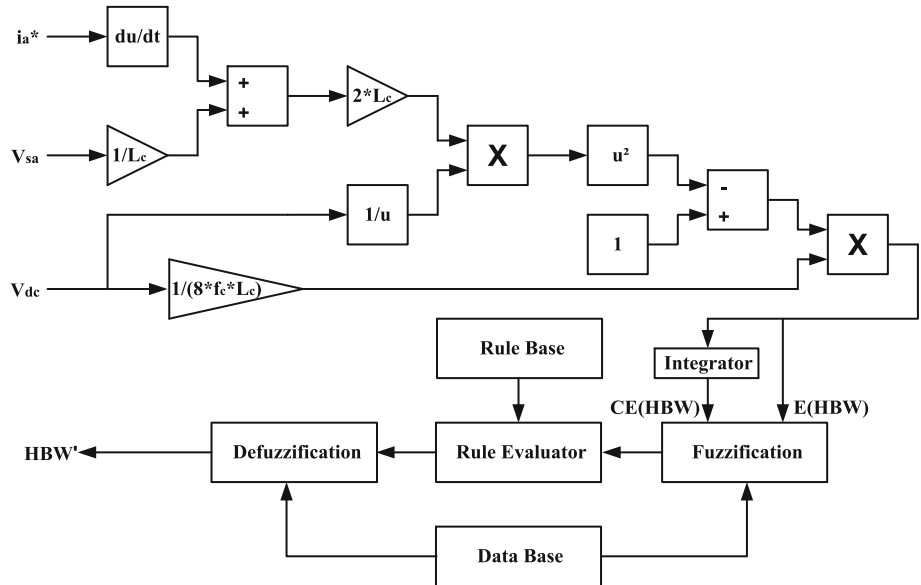


hysteresis current controller, 49 rules are formulated and are given in Table 1. The HBW′ is calculated by the proposed A-F-HCC is supposed to maintain a constant modulation frequency $f_c$. This A-F-HCC improves the performances of the HSAPF by reducing losses in the switching of the inverter to a large extent.

## 6 Results analysis

The investigations of the performance of proposed HSAPF are presented in this section under steady state and transient operating scenarios.

### 6.1 Simulated result analysis

In this case study, a shunt passive filter is designed based on the characteristic of the load. For better harmonic filtering, a SAPF is appended to the existing shunt passive filter system. A MOSFET-based inverter is modeled for

SAPF, and a capacitor is connected on its dc side for energy storage during transients. The control of the APF is done by dc link capacitor voltage regulation using PI or fuzzy logic controller. The switching pulse is generated by three different techniques such as HCC, A-HCC and A-F-HCC. For designing the passive filters, the reactive power requirement is taken as 2kVAR which is divided as 1000VAR for single-tuned 5th harmonic filter and 500VAR each for single-tuned 7th harmonic filter and double-tuned filter. A 3-Ø bridge rectifier with R-L load on its DC side is taken as the nonlinear load. Actually, when the load is diode rectifier, it does not require much reactive power, but for design purpose it is taken as such. The proposed power system incorporated with HSAPF model is developed in Matlab/Simulink. The various parameters of the hybrid filter system are tabulated in Table 2. First, the power system with the nonlinear load simulated without any filter and the wave shape of the load current along with its harmonic spectrum is depicted in Fig. 11. The load current is observed to be distorted having a total harmonic

**Table 2** Parameters of hybrid filter

| Parameters | Values |
| --- | --- |
| Source voltage ($V_{rms}$) | 230 V |
| System frequency ($f$) | 50 Hz |
| *Source impedances* | |
| Resistance ($R_s$) | 0.1 Ω |
| Inductance ($L_s$) | 0.5 mH |
| *Nonlinear load* | |
| Diode rectifier | 6-diode |
| Resistance ($R_L$) | 40 Ω |
| Inductance ($L_L$) | 100 mH |
| *Shunt active power filter* | |
| Power converter | 6-MOSFETs/6-diodes |
| Filter resistance ($R_c$) | 0.4 Ω |
| Filter inductance ($L_c$) | 1.35 mH |
| DC link capacitance ($C_{dc}$) | 2000 μF |
| Reference voltage ($V_{dc,ref}$) | 680 V |
| *Shunt passive power filter* | |
| 5th harmonic filter | kVAR = 1, quality factor $Q = 50$ |
| 7th harmonic filter | kVAR = 0.5, quality factor $Q = 50$ |
| 11th and 13th harmonic filter | kVAR = 0.5, quality factor $Q = 50$ |
| *PI controller* | $K_P = 0.35$, $K_I = 15$ |

distortion (THD) of 25.14% with dominant 5th, 7th, 11th and 13th harmonics. For the same load, analysis is performed in two different cases; Case I: when passive filter is connected alone and Case II: when both passive and active filters (HSAPF) are connected together.

**Case I**  When passive filter is connected alone.

In this case study, the harmonic mitigation is analyzed when shunt passive filter is incorporated with the power system. The source current and its frequency spectrum is

depicted in Fig. 12 from which it is analyzed that the THD is decreased from 25.14% to 17.50% and the harmonic contents are reduced with the effect of the passive filter. The source voltage, current, load current and the filter current are depicted in Fig. 13.

**Case II**  When hybrid filter is connected.

The mitigating ability of the hybrid filter consisting of both active and passive filters is presented here in this case study. The compensation by SAPF is achieved by the estimation of reference current effectively by using PI or FLC and the PWM switching pulse generation by using HCC or A-HCC or A-F-HCC techniques. In fixed hysteresis, the switching losses are very high and thus to overcome this and improve the PWM performance, a new A-F-HCC concept is used here to calculate the hysteresis bandwidth by FLC.

The wave shape of the source current along with its harmonic spectrum using A-F-HCC-HSAPF is shown in Fig. 14. From Fig. 14a–b, it is clear that THD is decreased from 17.50 to 2.25% and from 17.50 to 2.15%, respectively by using PI- and FLC-based HSAPF. Figure 15 presents the load current, source voltage, current, active and passive filter currents and the dc link voltage using the proposed A-F-HCC-based passive, active and HSAPF at steady state. From Fig. 15a, the source voltage is analyzed to be balanced because of the action of the passive filter. Figure 15b shows the source current without compensation or the load current. The injected passive filter current to the PCC is shown in Fig. 15c. Balanced and sinusoidal source current, injected current from the filter and the regulated dc side capacitor voltage is depicted in Fig. 15d–f and g–i, respectively, using A-F-HCC-based active and HSAPF. From Fig. 15f and i, it is shown that the capacitor voltage is regulated at 680 V and the proposed A-F-HCC-HSAPF decreases the settling time and percentage overshoot as compared to that of PI-based HSAPF. The settling time ($t_s$)

**Fig. 11** Wave shape of the load current along with its harmonic spectrum without any filter
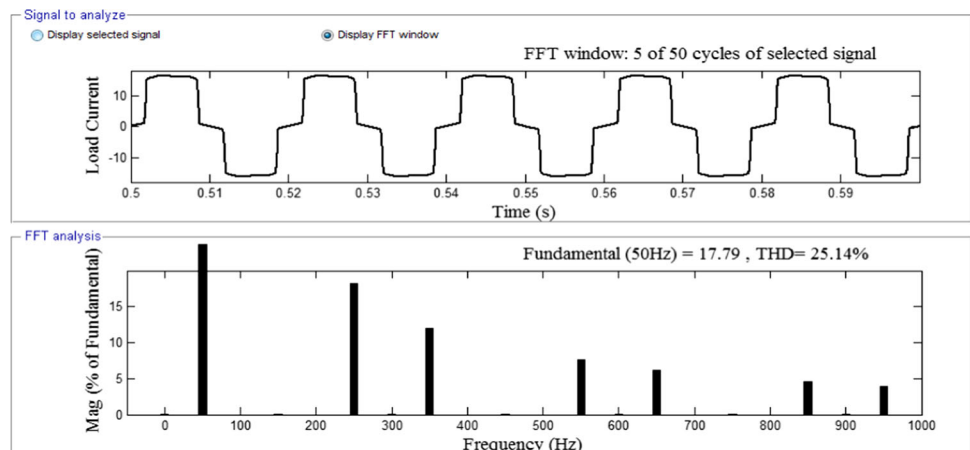
**Fig. 12** Wave shape of the source current and its harmonic spectrum using only passive filter
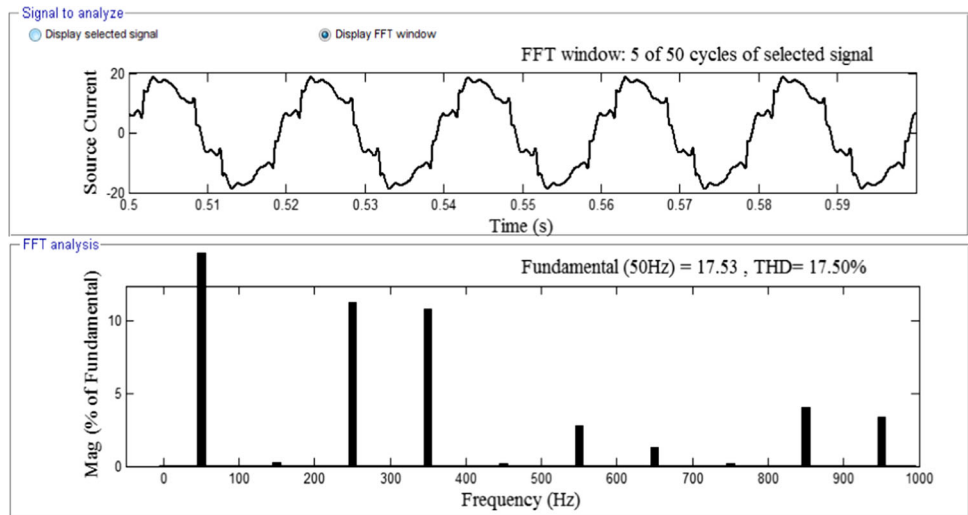


**Fig. 13** Various waveforms using only passive filter
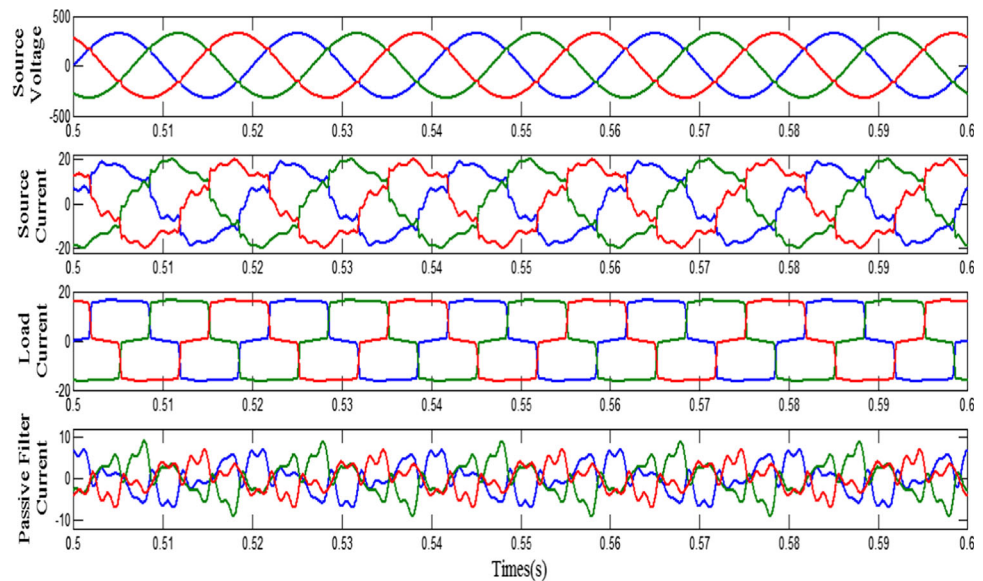


and percentage overshoot (%OS) of the dc link capacitor voltage are calculated under different PWM current control methods and are given in Table 3.

Figure 15j displays the voltage and current of phase-a in which the proposed A-F-HCC-HSAPF performs power factor improvements and simultaneously reduces the reactive power supplied from the source that improves the PQ of the system. Real power ($P$), reactive power ($Q$) and the power factor (CosØ) of the system are represented in Table 3 for different filters. Comparison of THD values is given in Table 3 from which it is analyzed that the THD in

the case of the proposed A-F-HCC-HSAPF is reduced to 2.15% as compared to that of the other filters.

### 6.1.1 Dynamic response of A-F-HCC-HSAPF system

To test the dynamic behavior of the A-F-HCC-HSAPF, a load change is applied in the simulation at 0.15 s (load is increased) and 0.3 s (load is decreased). At $t = 0.15$ s, the capacitor voltage is dropped when the load current is suddenly increased from 16.5 amps (peak value) to 30.00 amps and is recovered by the increase in the source current eventually. The transient response at this condition is

**Fig. 14** The wave shape of the source current along with its harmonic spectrum for HSAPF system **a** A-F-HCC with PI, **b** A-F-HCC with FLC
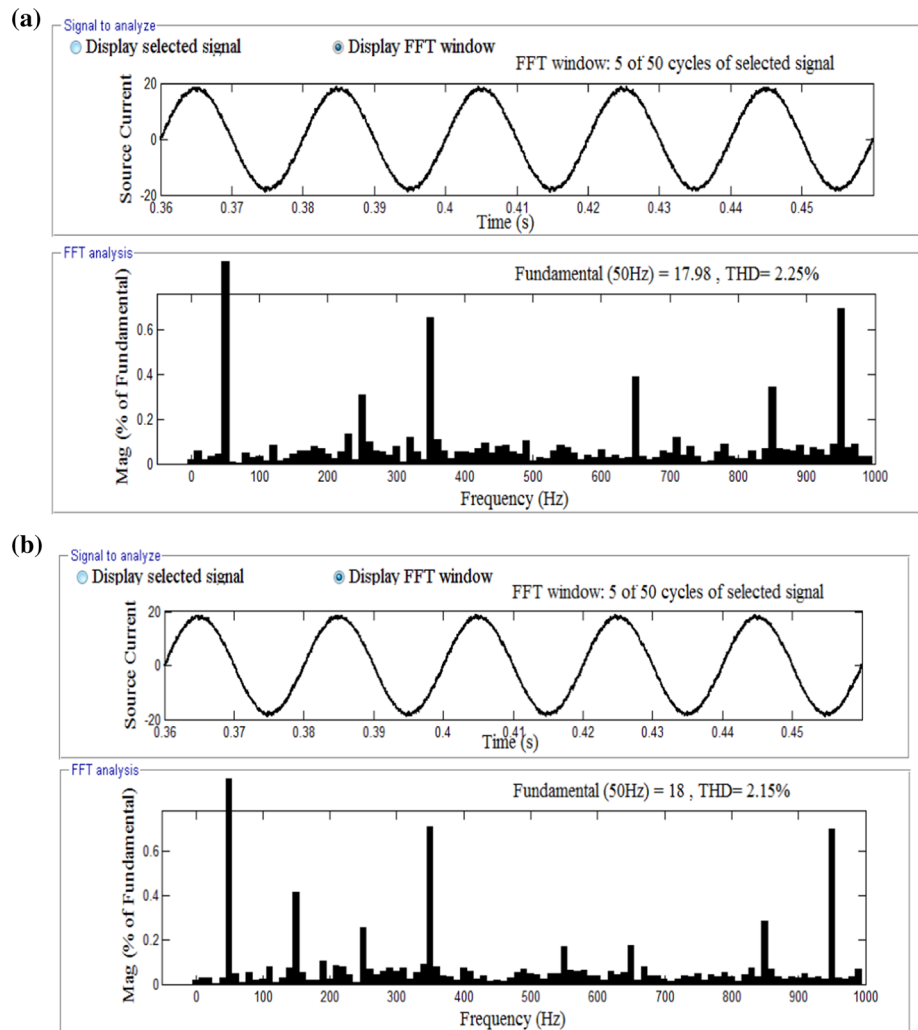
depicted in Fig. 16. For verifying the switch in response of A-F-HCC-HSAPF, the passive filter is connected in the line at 0.1 s and the active filter is connected at 0.2 s and the corresponding response is depicted in Fig. 17.

From Fig. 16, it is analyzed that the filter is effectively tracking the load changes and settled at a new steady state value. It is seen from the obtained results that APF is settling within 80 ms which is within four cycles. The active filter is generating a new filter current so that the source current becomes sinusoidal. Similar response is obtained when the active filter is switched at 0.1 s which is displayed in Fig. 17.

## 6.2 Experimental result analysis

The experiment setup to test the proposed A-F-HCC-HSAPF in the laboratory is shown in Fig. 18a. A model of SHAPF with 3 kW load is developed experimentally in

laboratory for testing the performance of the proposed controller under different operating scenarios. A real-time digital signal processing device (dSPACE, DS1103) is used along with CP1103 for signal analysis of the control algorithm. For designing the SHAPF system, SEMIKRON inbuilt IGBT-based inverter stack with all the supporting equipments is utilized. The voltages at the PCC, DC link and supply side is measured with the help of Hall Effect voltage (LV-25) sensor while the load point and source point currents are measured by the current sensors (LA-55p). These signals are being passed through the ADCs of DSP. The control signals produced by different controllers are fed through the IGBT's driver circuit. The recording and analyses of the signals are done with the help of Fluke power quality analyzer and digital storage oscilloscope (DSO). The specifications of the hardware components are given in Table 4.

**Fig. 15** Wave shape of A-F-HCC-HSAPF system at steady state **a** source voltage, **b** source current, **c** passive filter current using passive filter, **d** source current, **e** active filter current **f** dc link voltage using active filter, **g** source current **h** filter current, **i** dc link voltage using hybrid filter, **j** source voltage/current after compensation using proposed hybrid filter
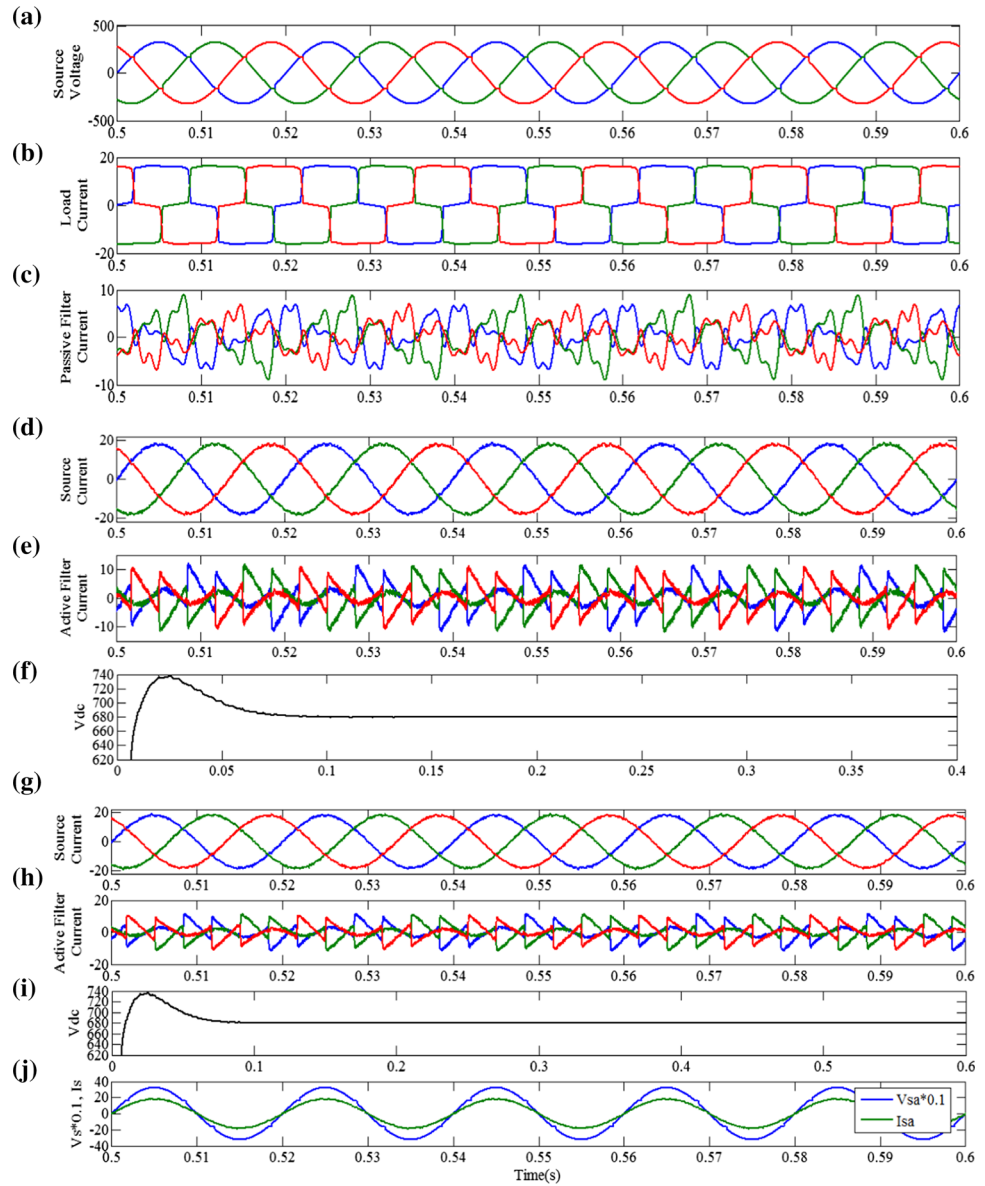


**Table 3** Various results under different condition

| Different condition | $t_s$ (s) | OS (%) | $P$ (kW) | $Q$ (VAR) | cosØ | THD (%) |
|---|---|---|---|---|---|---|
| Without any filter | – | – | 8.609 | 581.3 | .9673 | 25.1 |
| With passive filter | – | – | 8.372 | − 1572 | .9679 | 17.5 |
| HCC-PI-HSAPF | .11 | 8.66 | 8.772 | 30.12 | .9891 | 3.48 |
| HCC-F-HSAPF | .10 | 8.34 | 8.997 | 34.67 | .9912 | 3.07 |
| A-HCC-PI-HSAPF | .09 | 7.93 | 9.013 | 20.11 | .9918 | 2.93 |
| A-HCC-F-HSAPF | .09 | 7.81 | 9.114 | 20.34 | .9908 | 2.60 |
| A-PI-HCC-HSAPF | .07 | 7.69 | 9.334 | 17.65 | .9988 | 2.25 |
| A-F-HCC-HSAPF | .06 | 7.69 | 9.500 | 14.99 | .9990 | 2.15 |

**Fig. 16** Dynamic response of A-F-HCC-HSAPF for load change
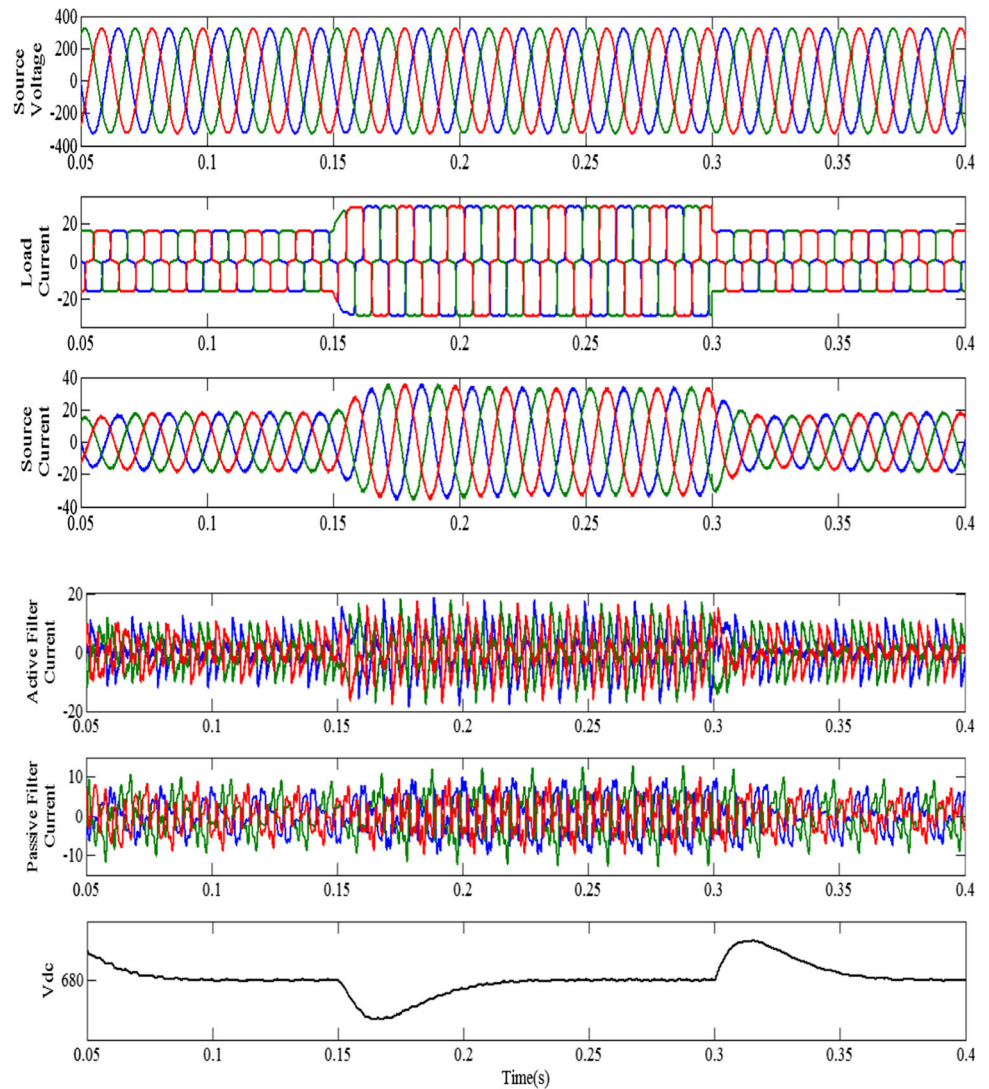


Figure 18b–e shows the three-phase source voltage, current, its harmonic spectrum and the performance parameters, respectively, without any filter. Figure 18b, c shows the three-phase source voltage, current are non-sinusoidal in nature because of the load nonlinearity. Frequency spectrum as shown in Fig. 18d consists of significant 5th, 7th, 11th and 13th harmonics and hence the THD of the three-phase currents are found to be 29.2%, 28.4%, 27.8%, respectively, for phases a, b, c, respectively. The power and power factor before filtering are depicted in Fig. 18e. Now to improve the system performance, A-F-HCC-HSAPF is connected to the system. Figure 19a and b gives the three-phase source current of the hybrid filter system and the harmonic spectrum of phase-a current, respectively. THD of the source current is observed to be decreased from 29.2 to 3.3% because of the compensating action of the proposed SHAPF. The filter current is presented in Fig. 19d. Further, the active, reactive powers, power factor (p. f.) and other performance parameters are shown in Fig. 19c. Here, the power factor is improved to 0.99 in the case of the proposed filter as compared to that without filter case with p. f. of 0.95.

# 7 Conclusion

In this research work, to test the robustness of the proposed fuzzy and conventional PI-based HSAPF, different case studies are performed under different scenarios. The

**Fig. 17** A-F-HCC-HSAPF
systems switch in response
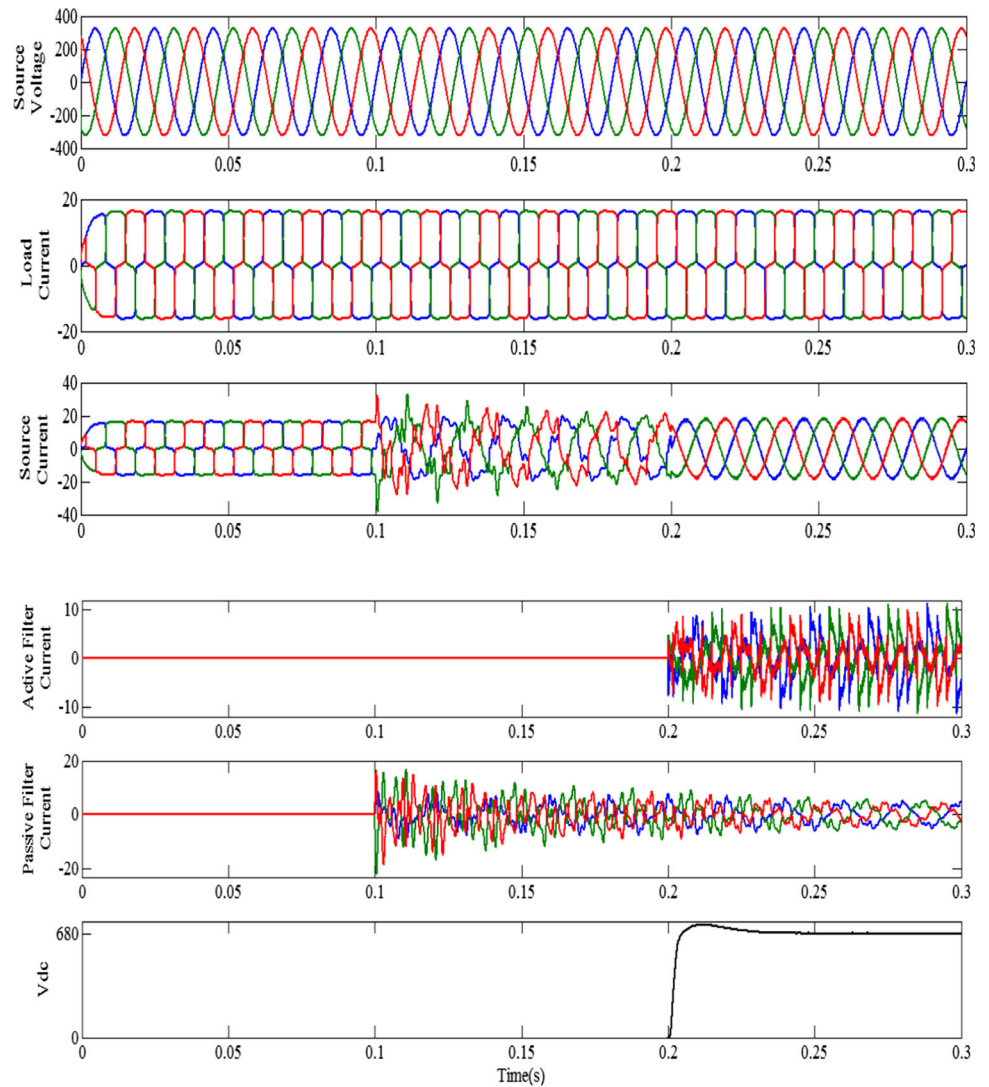


harmonic compensation performance is not satisfactory in the case of only passive filter as the THD is 17.50% in comparison to 25.14% in the case without any filter. Hence, SAPF is appended to the existing passive filter to design HSAPF. The estimation of reference current and regulation of voltage across dc link capacitor are done using PI or FLC. A-F-HCC is employed for generating the switching pulse of inverter. This technique is proposed in this paper for regulating the modulation frequency, to reduce the switching loss and to design an adaptive hysteresis band. Simulation and real-time case studies are carried out to investigate the mitigating capability of the proposed and other filters. From the result analysis, it is observed that the proposed A-F-HCC-HSAPF provides the enhanced harmonic compensation performance and minimum THD under all operating scenarios. It is within the IEEE-519 standard which is less than 5%.

In the future study, the stabilization of the dc link capacitor voltage can be achieved by connecting renewable energy resources such as solar PV, wind along with storage systems like battery, flywheel and ultra capacitors. The estimation of the reference can be done using some advanced nonlinear techniques like extended Kalman and adaptive filters for generating the suitable switching pulses to the inverters for achieving improved harmonics mitigation objective.

**Fig. 18** **a** Hardware experimental setup, **b** source voltage, **c** source current, **d** THD of phase-a source current, **e** performance parameters without any filter
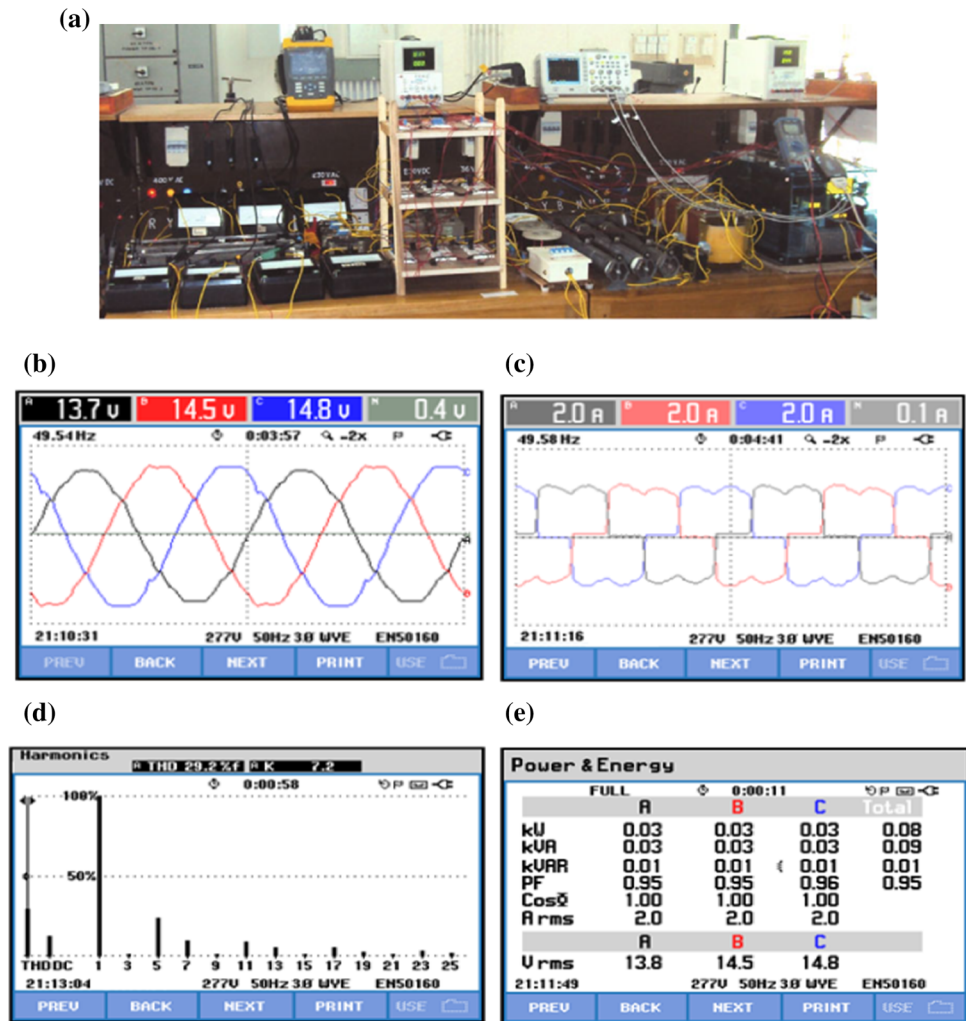


**Table 4** Experimental parameters

| Parameters | Value |
| --- | --- |
| Line voltage, frequency | 415 V, 50 Hz |
| Line, load impedances | $L_s = 0.15$ mH, $L_{ac} = 1.5$ mH, $R_L = 60\ \Omega$, $L = 10\ \mu$F; ($R_1 = 2\ \Omega$, $R_2 = 4\ \Omega$, $R_3 = 6\ \Omega$) |
| Tuned passive filter | $C_{f5} = 50\ \mu$F; $L_{f5} = 8.10$ mH; $C_{f7} = 20\ \mu$F; $L_{f7} = 8.27$ mH; $C_{f11} = 20\ \mu$F; $L_{f11} = 8.30$ mH |
| APF | $C_D = 1500\ \mu$F; $V_D = 750$ V |
| Coupling inductance | 5 mH |
| PI gains | $K_P = 0.5$, $K_I = 0.1$ |
| d-SPACE parameters (dSpace-DS1103) | Connector panel module—CP1103 |
| | MOSFET modules—SKM75GB123D |
| | MOSFET drivers as SKHI 22AR |
| | voltage and current sensors: (LV-25 and LA-55p) |
| | PQ analyzer (Fluke 43 B) |

**Fig. 19 a** Source current,
**b** THD of phase-a source
current, **c** performance
parameters of the hybrid filter
system, **d** filter current
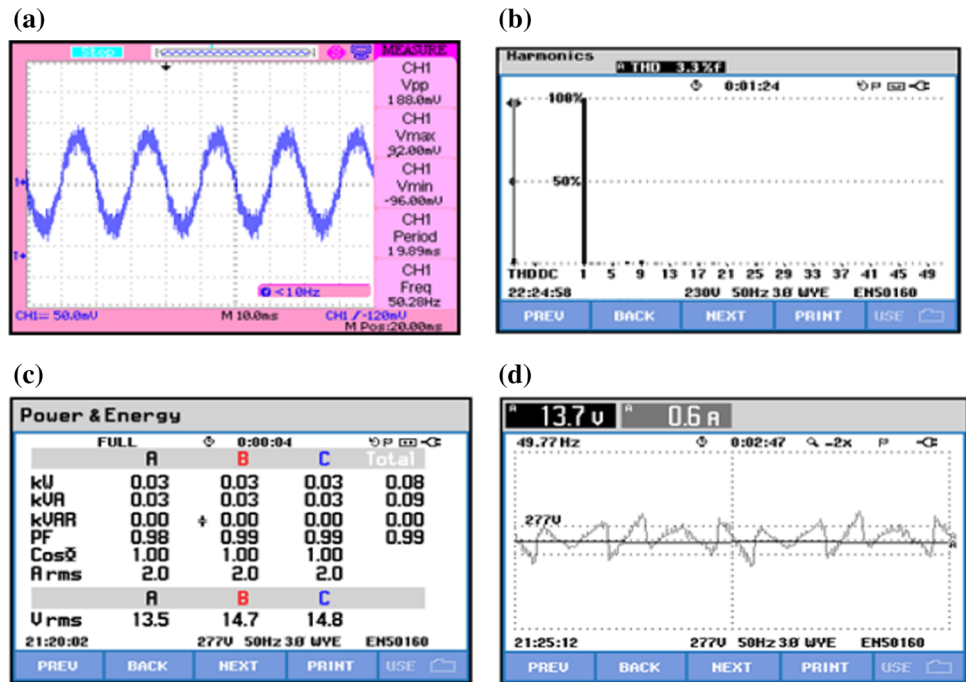


# References

1. Fuchs EWF, Masoum MAS (2008) Introduction to power quality. Power quality in power systems and electrical machines, 2nd edn. Academic Press is an imprint of Elsevier, Cambridge, pp 04–67

2. Busarello TDC, Pomilio JA, Simões MG (2016) Passive filter aided by shunt compensators based on the conservative power theory. IEEE Trans Ind Appl 52(4):3340–3347

3. Mahela OP, Shaik AG (2016) Topological aspects of power quality improvement techniques: a comprehensive overview. Renew Sustain Energy Rev 1(58):1129–1142

4. Carpinelli G, Proto D, Russo A (2017) Optimal planning of active power filters in a distribution system using trade-off/risk method. IEEE Trans Power Deliv 32(2):841–851

5. Bayındır KÇ, Cuma MU, Tümay M (2006) Hierarchical neuro-fuzzy current control for a shunt active power filter. Neural Comput Appl 15(3–4):223–238

6. Mahmoudian M, Gitizadeh M, Rajaei AH, Tehrani VM (2019) Common mode voltage suppression in three-phase voltage source inverters with dynamic load. IET Power Electron 12(12):3141–3148

7. Yunus HI, Bass RM (1996) Comparison of VSI and CSI topologies for single-phase active power filters. In: PESC Record. 27th annual IEEE power electronics specialists conference, vol 2, pp 1892–1898

8. Bhattacharya S, Frank TM, Divan DM, Banerjee B (1998) Active filter system implementation. IEEE Ind Appl Mag 4(5):47–63

9. Akagi H, Kanazawa Y, Nabae A (1984) Instantaneous reactive power compensators comprising switching devices without energy storage components. IEEE Trans Ind Appl 20(3):625–630

10. Peng FZ, Ott GW, Adams DJ (1998) Harmonic and reactive power compensation based on the generalized instantaneous reactive power theory for three phase four wire system. IEEE Trans Power Electron 13(6):1174–1181

11. Herrera RS, Salmeron P (2009) Instantaneous reactive power theory: a reference in the nonlinear loads compensation. IEEE Trans Ind Electron 56(6):2015–2022

12. Karimi H, Karimi-Ghartemani M, Iravani MR (2003) An adaptive filter for synchronous extraction of harmonics and distortions. IEEE Trans Power Deliv 18(4):1350–1356

13. Forghani M, Afsharnia S (2007) Online wavelet transform-based control strategy for UPQC control system. IEEE Trans Power Deliv 22(1):481–491

14. Tümay M, Meral ME, Bayindir KÇ (2008) Extraction of voltage harmonics using multi-layer perceptron neural network. Neural Comput Appl 17(5–6):585–593

15. Singh B, Verma V, Chandra A, Al-Haddad K (2005) Hybrid filters for power quality improvement. IEE Proc-Gener Transm Distrib 152(3):365–378

16. Kim S, Enjeti PN (2002) A new hybrid active power filter (APF) topology. IEEE Trans Power Electron 17(1):48–54

17. Oualid A, Moulahoum S, Colak I, Babes B, Kabache N (2016) Analysis, design and real-time implementation of shunt active power filter for power quality improvement based on predictive direct power control. In: 2016 IEEE international conference on renewable energy research and applications (ICRERA), pp 79–84

18. Badoni M, Singh A, Singh B (2016) Comparative performance of wiener filter and adaptive least mean square-based control for power quality improvement. IEEE Trans Ind Electron 63(5):3028–3037

19. Ouchen S, Betka A, Abdeddaim S, Menadi A (2016) Fuzzy-predictive direct power control implementation of a grid connected photovoltaic system, associated with an active power filter. Energy Convers Manag 122:515–525

20. Panda AK, Patnaik N (2017) Management of reactive power sharing & power quality improvement with SRF-PAC based UPQC under unbalanced source voltage condition. Int J Electr Power Energy Syst 84(2017):182–194

21. Ray PK, Das SR, Mohanty A, Eddy FYS, Krishnan A, Gooi HB, Amaratunga GJ (2018) Improvement in power quality using hybrid power filters based on robust extended Kalman filter. In: 2018 19th international Carpathian control conference (ICCC). IEEE, pp 585–590

22. Pradhan M, Mishra MK (2018) Dual P-Q theory based energy-optimized dynamic voltage restorer for power quality

improvement in a distribution system. IEEE Trans Ind Electron 66(4):2946–2955

23. Kamel K, Laid Z, Abdallah K, Anissa K (2018) Comparative analysis on shunt active power filter based PQ control strategy using HCC, SPWM and SVPWM switching signal generation techniques. In: 2018 15th international multi-conference on systems, signals & devices (SSD), pp 936–940

24. Yan W, Hu J, Utkin V, Xu L (2008) Sliding mode pulse width modulation. IEEE Trans Power Electron 23(2):619–626

25. Das SR, Ray PK, Mohanty A (2018) Fuzzy sliding mode based series hybrid active power filter for power quality enhancement. Adv Fuzzy Syst 2018:1–8. https://doi.org/10.1155/2018/1309518

26. Elgammal AA, El-naggar MF (2016) MOPSO-based optimal control of shunt active power filter using a variable structure fuzzy logic sliding mode controller for hybrid (FC-PV-Wind-Battery) energy utilisation scheme. IET Renew Power Gener 11(8):1148–1156

27. Fang Y, Fei J, Ma K (2015) Model reference adaptive sliding mode control using RBF neural network for active power filter. Int J Electr Power Energy Syst 73:249–258

28. Rahman A, Radzi NF, Amran M, CheSoh M, Mariun A, Abd Rahim N (2016) Adaptive hybrid fuzzy-proportional plus crisp-integral current control algorithm for shunt active power filter operation. Energies 9(9):737

29. Musa S, Radzi MAM, Hizam H, Wahab NIA, Hoon Y, Zainuri MAAM (2017) Modified synchronous reference frame based shunt active power filter with fuzzy logic control pulse width modulation inverter. Energies 10(6):758

30. Mahanty R (2014) Indirect current controlled shunt active power filter for power quality improvement. Int J Electr Power Energy Syst 62:441–449

31. Karuppanan P, Mahapatra KK (2012) PI and fuzzy logic controllers for shunt active power filter—a report. ISA Trans 51:63–169

32. Ozkan IA, Herdem S, Saritas I (2017) FPGA-based self-organizing fuzzy controller for electromagnetic filter. Neural Comput Appl 28(9):2535–2543

33. Noshadi A, Shi J, Lee WS, Shi P, Kalam A (2016) Optimal PID-type fuzzy logic controller for a multi-input multi-output active magnetic bearing system. Neural Comput Appl 27(7):2031–2046

34. Shi Kaibo, Zhong Shouming, Tang Yuanyan, Cheng Jun (2019) Non-fragile memory filtering of TS fuzzy delayed neural networks based on switched fuzzy sampled-data control. Fuzzy Sets Syst. https://doi.org/10.1016/j.fss.2019.09.001 (article in press)

35. Mukherjee M, Banerjee A (2019) Power quality improvement by active shunt filter with hysteresis current controller. In: Bera R, Sarkar S, Singh O, Saikia H (eds) Advances in communication, devices and networking. Springer, Singapore, pp 89–97

36. Kale M, Karabacak M, Saracoglu B (2013) A novel hysteresis band current controller scheme for three phase AC chopper. Int J Electr Power Energy Syst 44(1):219–226

37. Vahedi H, Sheikholeslami A, Tavakoli BM, Vahedi M (2011) Review and simulation of fixed and adaptive hysteresis current control considering switching losses and high-frequency harmonics. Adv Power Electron 2011:1–6. https://doi.org/10.1155/2011/397872